Chinese Journal of Structural Chemistry

ARTICLE

One-Pot Synthesis of Bismuth Basic Nitrate-Bi_2MoO_6 Photocatalyst for Selective Oxidation of Toluene

Tian-Qin Zeng[1], Lang Chen[1,2]*, Bing-Hao Wang[1], Sheng Tian[1], Zhang-Jun Bai[1], Xiong Wang[1], Jun-Kang Guo[1]* and Shuang-Feng Yin[1]*

[1]*Advanced Catalytic Engineering Research Center of the Ministry of Education, College of Chemistry and Chemical Engineering, State Key Laboratory of Chemo/Biosensing and Chemometrics, Hunan University, Changsha 410082, China*

[2]*College of Chemistry and Chemical Engineering, Jishou University, Jishou 416000, China*

ABSTRACT The key issues to improve the performance of photocatalysts for selective oxidation of toluene are promoting the migration and separation of charge carrier, and enhancing the generation of active oxygen species. It is known that the construction of compact heterojunction is an efficient protocol to inhibit photogenerated electron-hole recombination. In this work, a 2D-2D $[Bi_6O_6(OH)_3](NO_3)_3{\cdot}1.5H_2O$-$Bi_2MoO_6$ (denoted as BBN-BMO) composite heterojunction has been prepared by one-step hydrothermal method for the first time. The tetragonal phase BBN in the composite plays the role of transferring electrons from the visible light activated orthorhombic phase BMO and promoting the generation of active $\bullet O_2^-$, the holes left in BMO are used to activate toluene and produce benzyl radical, thus greatly improving the photocatalytic performance for selective oxidation of toluene. The toluene conversion rate of BBN-BMO is 3466 $\mu mol{\cdot}g^{-1}{\cdot}h^{-1}$, which is three times that of pure BMO. The selectivity to benzaldehyde is 94.2%. In addition, reasonable mechanism has been speculated based on a series of control experiments.

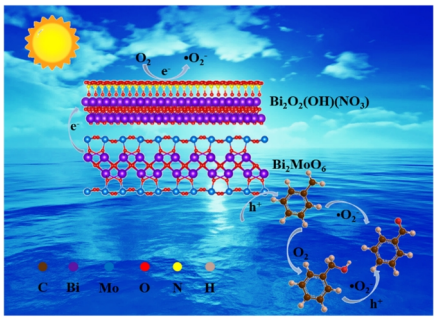

Keywords: Bi_2MoO_6, basic bismuth nitrate, heterojunction, photocatalysis, selective oxidation of toluene

n INTRODUCTION

Toluene has been mainly obtained from crude oil through petrochemical process, which is commonly used as solvent in chemical processes. However, it can also act as a resource in organic synthesis. For example, selective oxidation of the C(sp^3)-H bond of toluene to generate benzyl alcohol, benzaldehyde or benzolic acid has been an effective route to elevate the economic value of toluene.[1,2] Among them, benzaldehyde has been widely used in the synthesis of fine chemicals and materials, including pharmaceuticals, spices, pesticides, detection reagents and so on.[3,4] However, the traditional processes for benzaldehyde production are suffering from organochloride residual or harsh reaction conditions, such as high temperature and high pressure, which limits the application of benzaldehyde product and improves the cost of production.[5,6] Therefore, it is of great significance to prepare benzaldehyde from toluene in a mild and eco-friendly way. The photocatalytic protocol has been proved to be a promising alternative, because of its utilization of oxygen as green oxidant. In addition, high selectivity of benzaldehyde can be achieved at mild condition.[7-11] Until now, many kinds of catalysts have been reported in this field, including TiO_2,[12] CdS,[13] halide perovskite,[14] BiOX,[15,16] Bi_2WO_6,[17] metal organic frameworks (MOFs)[18], etc. However, there are still shortcomings, such as insufficient light utilization efficiency, poor stability, low conversion rate of toluene, and unsatisfactory selectivity of benzaldehyde.[19-23]

Aurivillius Bi_2MoO_6 (BMO), with good visible light absorption capacity and suitable band gap structure, has shown potential applications in photocatalytic oxidation of toluene into benzaldehyde.[24,25] However, the photocatalytic performance would be greatly limited by the serious charge carrier recombination and insufficient active sites on the surface.[26] In order to solve these problems, some strategies have been developed, such as element doping, defect engineering and heterojunction construction.[27-29] Among them, the construction of appropriate heterojunction can achieve the rapid migration of photogenerated electrons or holes, thus effectively inhibiting the recombination of photogenerated carriers. In addition, the redox capacity of catalytic materials can be effectively regulated.[30-32] In our previous work, Bi ion self-doped Bi_2MoO_6-$Bi_2Mo_3O_{12}$ heterojunction was fabricated by a one-step hydrothermal method with $Bi_{3.64}Mo_{0.36}O_{6.55}$ as the precursor.[24] The compact heterojunction improved the separation efficiency of optical carriers, and the doped Bi adjusted the redox capacity of each component. Meanwhile, 0D/2D heterojunction was constructed by adding appropriate TiO_2 nanoparticles to trap photogenerated electrons from BMO, so as to improve its photocatalytic activity.[33] $[Bi_6O_6(OH)_3](NO_3)_3{\cdot}1.5H_2O$ (BBN) is a product of incomplete hydrolysis of bismuth nitrate, which is of benefit for the construction of compact heterojunction with other Bi-containing semiconductors.[34,35] Therefore, the construction of $[Bi_6O_6(OH)_3](NO_3)_3{\cdot}1.5H_2O$-$Bi_2MoO_6$ (BBN-BMO) compact heterojunctions by one-pot method is assumed to be reasonable, in which the BBN will act as electron trap according to its unique band gap structure.

In this work, a series of 2D-2D compact BBN-BMO heterojunction materials were prepared by a simple hydrothermal method, with adjusted ratio of $Bi(NO_3)_3{\cdot}5H_2O$ and molybdenum sources. Attributed to its *in-situ* grown heterostructure, photogenerated electrons can be easily transferred by BBN for reducing adsorbed O_2 into active $\bullet O_2^-$. The optimal BBN-BMO-160 can achieve ex-

DOI: 10.14102/j.cnki.0254-5861.2022-0149

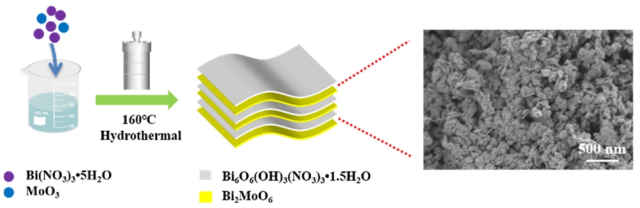

Scheme 1. The preparation process of BNN-BMO and SEM image of BBN-BMO-160.

cellent performance for benzaldehyde formation.

n RESULTS AND DISCUSSION

$[Bi_6O_6(OH)_3](NO_3)_3·1.5H_2O$-$Bi_2MoO_6$ composites (BBN-BMO-x, x = 140, 160 and 180) were prepared by a hydrothermal method (Scheme 1), using MoO_3 and $Bi(NO_3)_3·5H_2O$ as resources. From the XRD patterns, one can see that all diffraction peaks of obtained BBN and BMO match well with those of tetragonal phase BBN (PDF#53-1038) and orthorhombic phase BMO (PDF#21-0102), respectively, without other detected impurity (Figure 1a). In the diffraction pattern of BBN-BMO-160, we can clearly see the characteristic peaks belonging to BBN (10.2°, 25.4°, and 31.3°) and BMO (28.1°), respectively, thus confirming the formation of BBN-BMO heterojunction. From the diffraction patterns of BBN-BMO samples prepared at different temperatures, the crystallinity of BBN is found gradually increased with the rising temperature (Figure 1b). Disclosing with their photocatalytic performance, we speculate that appropriate crystallinity of BBN might be more conducive to the photocatalytic performance for toluene oxidation (vide infra).

X-ray photoelectron spectroscopy (XPS) was applied to study the chemical states of elements on the surface of prepared samples. All elements (Bi, Mo, O, N) belonging to BMO and BBN in BBN-BMO-160 can be found (Figure 1c-f). The Bi 4f spectrum of BBN-BMO-160 can be divided into four obvious peaks (158.42, 159.42, 163.79, and 164.71 eV) and two small peaks (157.46 and 163.16 eV). The two peaks located at 158.42 and 159.42 eV are assigned to Bi $4f_{7/2}$, and the other two at 163.79 and 164.71 eV are corresponding to Bi $4f_{5/2}$ of Bi^{3+}, respectively. The two small peaks (157.46 and 163.16 eV) indicate the low state of dangling Bi, which may be related to the oxygen vacancy on the surface of the material.[36] The spectrum of O 1s can be divided into three peaks at 529.78, 530.83 and 532.97 eV, corresponding to the lattice oxygen of Bi-O layer,[34] the adsorbed oxygen, and the NO_3^- contained in the catalytic material, respectively.[37] In the Mo 3d pattern of BBN-BMO-160, a pair of strong peaks located at 235.66 and 232.69 eV correspond to the oxidation state of Mo^{6+} reported in the literature, while the other two peaks (231.67 and 234.94 eV) are assigned to the low-valence state of Mo.[36] The N 1s peak at 406.11 eV in BBN-BMO shows a slight shift compared with that in BBN.[34] As can be seen from these figures, the binding energies of Bi 4f, O 1s, and Mo 3d in BBN-BMO-160 shift positively compared to that of pure BMO, while the Bi 4f, O 1s and N 1s have a certain negative displacement relative to BBN. It indicates strong interaction between BBN and BMO in the composites and the facile transfer of electrons from BMO to BBN at the interface of the heterojunction.[38,39]

Field emission scanning electron microscopy (FE-SEM) and high-resolution transmission electron microscopy (HR-TEM) were used to determine the morphology and microstructure of the prepared catalyst. As can be seen from Figure 2a-c, BBN presents a micro-size block structure, while BMO exhibits uneven nanoflake structure with relatively smooth surface. The BBN-BMO-160 presents as uniform nanosheet with rough surface, which is smaller than that of BMO, indicating the exposure of more active sites. The TEM images further confirm the small sheet-like structure of BBM-BMO-160 (Figures 2d and e). From the HR-TEM image, the lattice spacing measured at 0.328 nm corresponds to the lattice fringe of the (131) crystal plane of BMO,[31] while the different lattice spacing at 0.288 nm is contributed by the lattice fringe of the

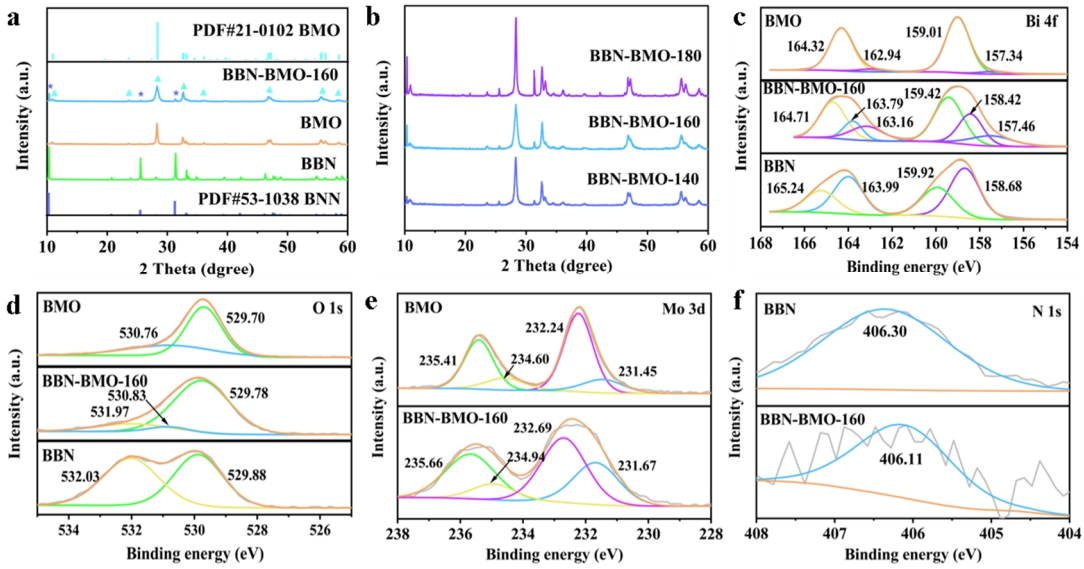

Figure 1. (a) XRD patterns of BBN, BMO, and BBN-BMO-160. (b) XRD patterns of BBN-BMO samples prepared at different temperatures. High resolution XPS spectra of (c) Bi 4f, (d) O 1s for BBN, BMO and BBN-BMO-160; (e) Mo 3d for BMO and BBN-BMO-160; (f) N 1s for BBN and BBN-BMO-160.

DOI: 10.14102/j.cnki.0254-5861.2022-0149

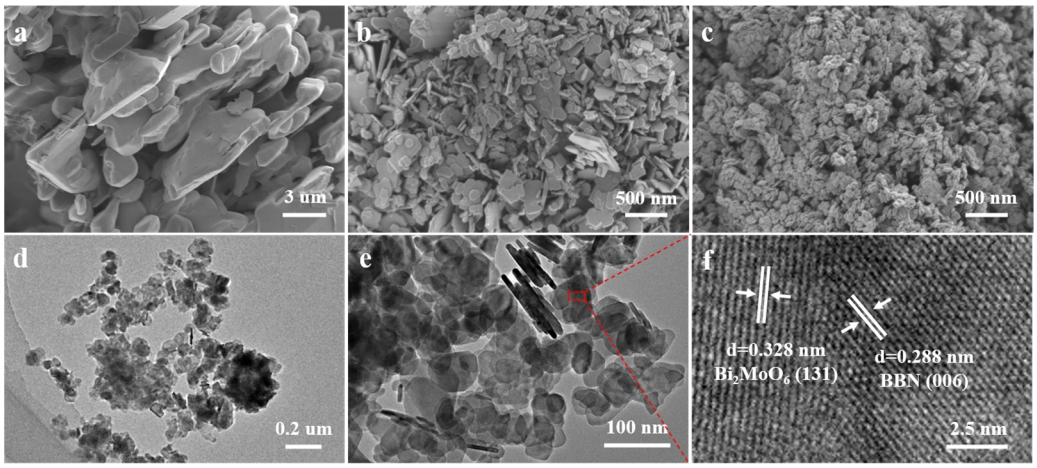

Figure 2. SEM images of (a) BBN, (b) BMO and (c) BBN-BMO-160. TEM (d, e) and HR-TEM (f) images of BBN-BMO-160.

(006) crystal plane of BBN.[34] Clearly, there is a close interface between BBN and BMO (named as heterojunction), which can effectively promote the migration and separation of photogenerated carriers.

According to the UV-vis diffuse reflectance spectroscopy (UV-vis DRS), the BMO can absorb visible light, while BBN can only absorb ultraviolet light. BBN-BMO-160 has a slight red shift relative to BMO (Figure 3a), indicating its good absorption capacity of visible light. The band gap of the samples is calculated by the Kubelka-Munk equation[13], and the E_g values of BBN and BMO are 3.52 and 2.75 eV, respectively (Figure 3b). Mott-Schottky (M-S) plots show positive slopes in the linear region, indicating that both BBN and BMO are n-type semiconductors (Figures 3c and d). Importantly, the flat band potentials of BBN and BMO are -0.12 and -0.25 V (vs. Ag/AgCl), respectively. The conversion potential of the conduction band (CB) (vs. Ag/AgCl) from the flat band (vs. Ag/AgCl) is generally considered to be ~0.30 V.[13,40-42] Therefore, the CB positions of BBN and BMO are -0.42 and -0.55 V (vs. Ag/AgCl), respectively. The corresponding CB positions are -0.22 and -0.35 V after conversion to standard hydrogen electrode (vs. NHE), which can meet the reaction potential of $O_2/\bullet O_2^-$ (-0.13 V).[17,43] Moreover, it can be speculated that photogenerated electrons could flow from BMO to BBN, thus promoting the migration and separation of carriers, which is consistent with the results of XPS analysis. Obviously, the valence band (VB) potentials of BBN and BNN are 3.30 and 2.40 eV (vs. NHE), as calculated by the formula ($E_{VB} = E_{CB} + E_g$).

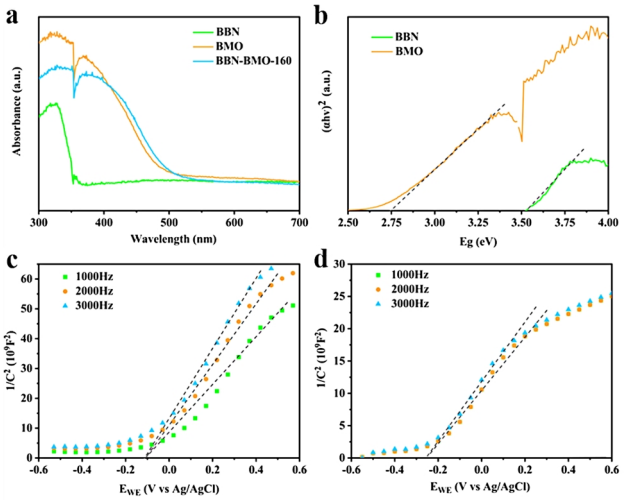

Figure 3. (a) UV-vis DRS spectra of BBN, BMO and BBN-BMO-160. (b) Tauc plots of BBN and BMO. Mott-Schotty (M-S) plots of (c) BBN and (d) BMO.

The separation of photogenerated electron and hole is the key to achieve good photocatalytic performance. To verify the charge carrier migration and separation ability of photocatalysts, the photoluminescence (PL) of the sample was tested with an excitation wavelength of 280 nm. As can be seen from Figure 4a, the emission peak intensity of BBN-BMO-160 is significantly weaker than that of BMO, indicating that the formation of BBN-BMO heterojunction can effectively inhibit the recombination of photogenerated carriers. In order to further analyze the carrier migration efficiency, photoelectrochemical measurements of the samples (Figure 4b) show that BBN-BMO-160 has a higher photocurrent response than that of its two components. In addition, BBN-BMO-160 has a smaller impedance diameter as can be seen from the electrochemical impedance (ESI) graph (Figure 4c). These results indicate that, the formation of BBN-BMO heterojunction is beneficial to separate electron and accelerate its migration in the composite sample.

Photocatalytic selective oxidation of toluene under visible light was used to evaluate the performance of photocatalytic materials (Figure 5). As can be seen, BBN-BMO-160 displays the best photocatalytic performance, with the benzaldehyde formation rate of 3265 $\mu mol \cdot g^{-1} \cdot h^{-1}$ and the selectivity of 94.2%. The formation rate of BBN-BMO-160 is about three times that of BMO, which is superior to most of the reported photocatalysts without solvent to data (Table S1). Because BBN can't utilize visible light, only trace amount of benzaldehyde is detected. It is shown that, light, O_2 and photocatalyst are indispensable for the selective oxidation of toluene. When pure O_2 is replaced by air as oxidant, the toluene conversion rate is decreased, further confirming that O_2 is oxidant in the reaction process. When the irradiation light is extended to UV region, the activity is increased, suggesting that exciting BBN

DOI: 10.14102/j.cnki.0254-5861.2022-0149

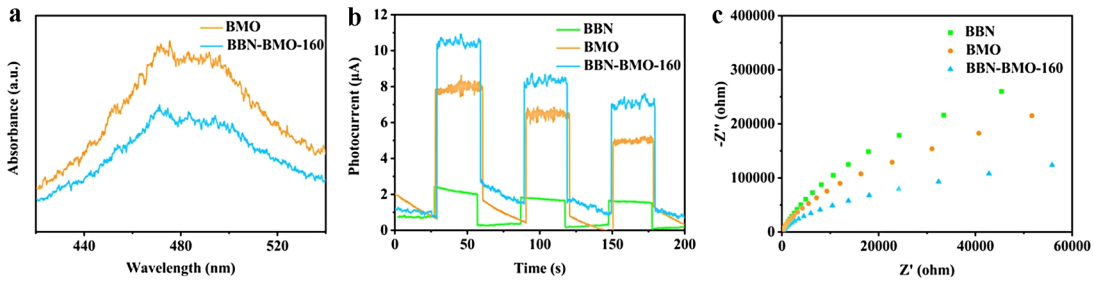

Figure 4. (a) PL spectra of BMO and BBN-BMO-160. (b) Transient photocurrent response and (c) ESI of BBN, BMO and BBN-BMO-160.

will enhance the generation of charge carriers. In addition, whether the hydrothermal temperature is increased or decreased, the activity of prepared composite is reduced. Based on the results of PL, photocurrent response and ESI, we believe that the formation of BBN-BMO compact heterojunction is the key to improve the photocatalytic toluene oxidation performance of BBN-BMO-160, which effectively inhibits the efficiency of photogenerated carrier recombination.

We studied the stability of BBN-BMO-160 catalyst. There is still high photocatalytic activity for toluene oxidation after three reaction cycles (Figure 6a). At the same time, we used XRD to mark the catalysts before and after reaction. There is no significant change in the crystal phase before and after reaction (Figure 6b). Therefore, we speculate that the slight decrease in activity might be caused by the inactivation of partial active sites of BBN-BMO-160.[17,34,38] To study the active species in the photocatalytic selective oxidation of toluene, control experiments were conducted. We conduct the reaction in presence or absence of oxygen, and add various trapping agents to capture the free radicals in the system. Then, the formation rate is determined (Figure 6c). In the vacuum, there is neither benzaldehyde nor benzyl alcohol detected, indicating that O_2 is indispensable in the selective oxidation process of toluene. When 2,2',6,6'-tetramethylpiperidine-1-oxyl (TEMPO) was added into the reaction system to quench all free radicals,[9,44] the photocatalytic activity is quenched obviously, indicating that the photocatalytic selective oxidation of toluene is a free radical-dependent process. When adding ammonium oxalate (AO) and potassium persulfate ($K_2S_2O_8$) as hole and electron trapping agents,[13,17,45] the catalytic activity is also greatly reduced, indicating both hole and electron are important for the reaction. It is known that the photogenerated electrons could reduce adsorbed O_2 into superoxide anion radicals ($\bullet O_2^-$), which can act as active oxygen species.[13,17] The formation of $\bullet O_2^-$ during the reaction was determined by electron spin resonance (ESR) (Figure 6d), using 5,5-dimethyl-1-pyrroline N-oxide (DMPO) as a trap agent.[11,46] No signal belonging to DMPO-$\bullet O_2^-$ is detected in dark, however, typical peaks appear after BBN-BMO-160 is exposed to light for 10 min, indicating that BBN-BMO-160 produces $\bullet O_2^-$ under aerobic and light conditions. However, when mannitol is added as the •OH catcher in the reaction,[25,47] there is almost no effect on the reaction, indicating that •OH is not involved in this process.

Based on the results discussed above, we propose a possible mechanism of photocatalytic selective oxidation of toluene over BBN-BMO-160 (Figure 7). As illustrated, the CB and VB of BBN and BMO are -0.22, 3.30 eV and -0.35, 2.40 eV, respectively. When BBN-BMO-160 catalyst is exposed under visible light, only BMO can be excited to generate electron-hole pairs. The electrons (e^-) in the CB of BMO are migrated to BBN along the heterojunction, and then combine with oxygen to generate $\bullet O_2^-$ because of their different CB potentials. Due to their difference of CB

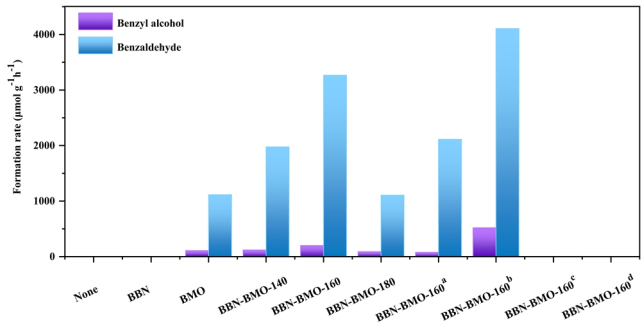

Figure 5. Performance of photocatalysts for toluene selective oxidation. Reaction condition: toluene (2 mL), photocatalyst (10 mg), O_2 (1 mL min^{-1}), light irradiation (300 W Xe lamp, λ > 400 nm), reaction time (3 h); [a] replacing O_2 by air; [b] light irradiation (300 W Xe lamp, λ > 330 nm); [c] without irradiation; [d] under vacuum.

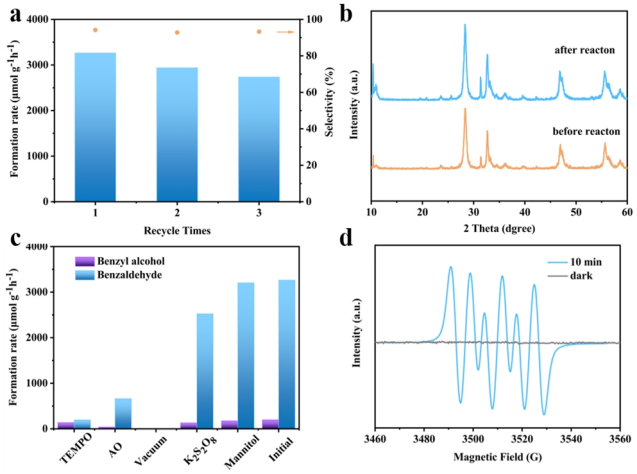

Figure 6. (a) Recycle property of BBN-BMO-160. (b) XRD patterns of BBN-BMO-160 before and after reaction. (c) Quenching experiments of toluene oxidation using 2,2',6,6'-tetramethylpiperidine-1-oxyl (TEMPO), mannitol, ammonium oxalate (AO), or potassium persulfate ($K_2S_2O_8$) as scavenger, respectively. (d) The 5,5-dimethyl-1-pyrroline N-oxide (DMPO) spin-trapping ESR spectra of BBN-BMO-160 for $\bullet O_2^-$ under visible-light irradiation for 10 min.

DOI: 10.14102/j.cnki.0254-5861.2022-0149

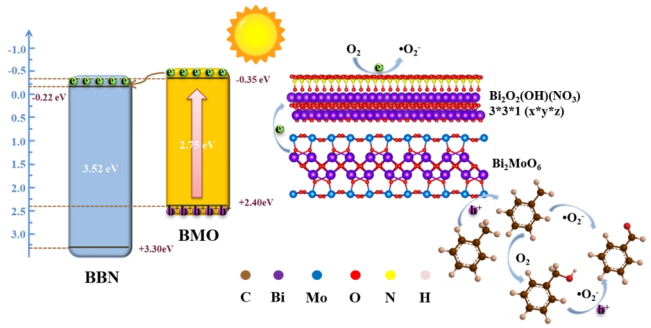

Figure 7. Proposed reaction mechanism for the photocatalytic oxidation of toluene over BBN-BMO-160.

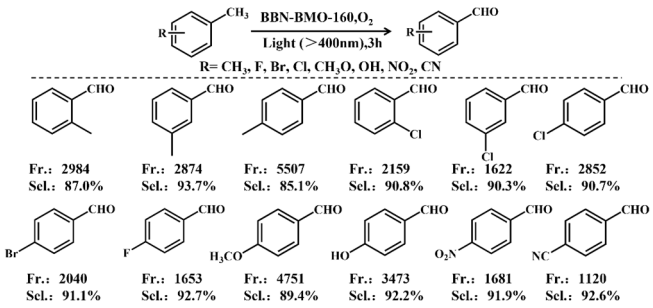

Figure 8. Substrate scope for the photocatalytic oxidation of aromatic alkanes. (Fr: formation rate in μmol·g^{-1}·h^{-1}, Sel: selectivity)

potentials, the electrons (e^-) in the CB of BMO are migrated to BBN along the heterojunction, and that of BBN is -0.22 V, which meets the reduction potential of O_2/•O_2^- (-0.13 V).[17,43] Thus it can combine with oxygen to form •O_2^-. At the same time, the hole (h^+) left in the VB of BMO dehydrogenates the adsorbed toluene molecules to form benzyl radicals, which then forms benzaldehyde through two pathways. Most of the benzyl radicals react with •O_2^- directly to generate benzaldehyde, while a small fraction reacts with oxygen to produce benzyl alcohol, which further reacts with h^+ and •O_2^- to form benzaldehyde.[8,13,48,49]

Some toluene derivatives were selected to further explore the substrate universality of BBN-BMO-160 as photocatalyst. As can be seen from Figure 8, BBN-BMO-160 reports a good to excellent activity towards all these substrates. For -CH_3 or -Cl at different substitution position, the benzaldehyde formation rate varies, and the highest activity is observed at the para-substituted one. By changing the para-substitution groups from -F, -Br, -CH_3O, -OH, -NO_2 to -CN, we find that the electron-giving groups can promote the oxidation of toluene to a certain extent, while the electron-absorbing groups can partially inhibit the reaction. The result is in agreement with the reported works, suggesting the breaking of C(sp^3)-H bond of toluene is the rate-determining step.[8,19]

n CONCLUSIONS

In this work, BBN-BMO photocatalyst with 2D-2D compact heterojunction was prepared for the first time and applied in photocatalytic selective oxidation of toluene. Attributed to the formation of compact heterojunction, photogenerated electrons of BMO can be easily transferred to BBN, and then reacted with adsorbed O_2 to produce active species (•O_2^-). Thus, under the irradiation of visible light with oxygen as oxidant, the formation rate of benzaldehyde of 3265 μmol·g^{-1}·h^{-1} is achieved. This work provides a reference for the facile one-pot synthesis of heterojunction photocatalysts.

n EXPERIMENTAL

Material and Reagents. $Na_2MoO_4·2H_2O$ (99%), $Bi(NO_3)_3·5H_2O$ (99%), and HCl (36-38 wt%) were purchased from Sinopharm Chemical Reagent Co., Ltd., and used without further purification. Deionized water (homemade) was used throughout the experiment.

Preparation of the MoO_3 Nanobelts. The MoO_3 nanobelts were prepared according to the reported method.[50] In a typical experiment, 10 mmol $Na_2MoO_4·2H_2O$ was added to 50 mL water and stirred for 5 min to completely dissolve, followed by the addition of appropriate amount of HCl to adjust the pH to 1. After stirring for 20 min, the mixture was transferred to a 100 mL Teflon-lined autoclave and reacted at 180 ℃ for 12 h. After being cooled down to room temperature, the product was collected by centrifuging, washed with deionized water for 4 times, and then dried in oven at 80 ℃ for 24 h.

Preparation of the BBN-BMO-x Photocatalyst. First, 1 mmol MoO_3 was added to 50 mL of water and ultrasound was performed for 15 min to form a uniform suspension. Then 2.5 mmol $Bi(NO_3)_3·5H_2O$ was added and stirred for 30 min. Afterwards, the mixed solution was transferred to a 100 mL Teflon-lined autoclave and reacted at different temperatures for 24 h.[51] After being cooled to room temperature, it was collected by centrifuging, washed with deionized water for 4 times, and then dried in an oven at 80 ℃ for 24 h. The achieved samples were named as BBN-BMO-x, where x indicated the reaction temperature (140, 160 and 180 ℃).

Preparation of the BMO Photocatalyst. First, 1 mmol MoO_3 was added to 50 mL of water and ultrasound was performed for 15 min to form a uniform suspension, then 2 mmol $Bi(NO_3)_3·5H_2O$ was added and stirred for 30 min. The mixed solution was then transferred to a 100 mL Teflon-lined autoclave and reacted at 160 ℃ for 24 h. After being cooled to room temperature, it was collected by centrifuging, washed with deionized water for 4 times, and then dried in an oven at 80 ℃ for 24 h.

Preparation of the BBN Photocatalyst. 2.5 mmol $Bi(NO_3)_3·5H_2O$ was added to 50 mL of water and stirred for 30 min. Then the mixed solution was transferred to a 100 mL Teflon-lined autoclave and reacted at 160 ℃ for 24 h. After being cooled to room temperature, it was collected by centrifuging, washed with deionized water for 4 times, and then dried in oven at 80 ℃ for 24 h.

n CHARACTERIZATION

The Characteristics. The phase structure of samples was characterized using the D8 Advance X-ray diffractometer with monochromatized Cu-Kα radiation (λ = 0.15406 nm). XPS spectra were collected by using a monochrome Al Kα ($h\nu$ = 1253.6 eV) X-ray source with Nexsa apparatus to characterize the types of ele-

DOI: 10.14102/j.cnki.0254-5861.2022-0149

ments on the surface and the oxidation states of the corresponding elements. All spectra were calibrated by using a contaminant carbon (C 1s = 284.8 eV) as a reference. The FE-SEM (JSM-7610FPlus) and HR-TEM (JEOL, JEM-2100Plus) were used to detect the morphology and structure of catalysts. ESR spectra were conducted at room temperature over a Bruker A200 spectrometer to test the production of reactive oxygen species during photocatalytic reactions. The UV-vis diffuse reflectance spectra (UV-vis DRS) of the catalyst powder state were collected using a Cary-100 spectrophotometer (Shimadzu, Japan). PL spectra were acquired on a Hitachi F-4600 spectrometer. All electrochemical measurements including transient photocurrent, Mott-Schottky (M-S) plots, and EIS was performed in a conventional three-electrode system using 0.5 M $NaSO_4$ as electrolyte. The samples coated with FTO (square 1 cm^2), Ag/AgCl (KCl), and platinum wire were used as working electrode, reference electrode, and counter electrode, respectively, and were collected in an electrochemical workstation (CHI660E, Chenhua Co. Ltd., Shanghai, China) at room temperature.

Photocatalytic Performance Evaluation. Briefly, 2 mL of toluene and 10 mg of photocatalyst were added to a 25 mL two-necked round-bottom flask fitted with a condensing reflux unit, and the oxygen flow (1 $mL \cdot min^{-1}$) was circulated into the mixture. In order to achieve the adsorption and desorption balance between the substrate and catalyst, as well as fully dissolving oxygen in the substrate, dark treatment was performed for 30 min before illumination. A 300 W Xe lamp (PLS-SXE 300 C, Perfectlight) with a 400 nm cut off filter was used as irradiation source. After 3 h of reaction at room temperature, the mixed solution was centrifuged to recover the solid catalyst, and the upper layer was analyzed by Shimadzu GC-2010Plus with a capillary SH-Rtx-1701 column, using n-decane as internal standard.

$$\text{Conversion rate} = \frac{\text{moles of toluene reacted}}{\text{time of reaction} \times \text{mass of catalyst}}$$

$$\text{Formation rate} = \frac{\text{moles of corresponding product}}{\text{time of reaction} \times \text{mass of catalyst}}$$

$$\text{Selectivity (\%)} = \frac{\text{moles of corresponding product}}{\text{moles of toluene reacted}} \times 100\%$$

n ACKNOWLEDGEMENTS

This research was financially supported by the National Natural Science Foundation of China (Nos. 21975069, 21725602, 22108067, and 21938002), the Innovative Research Groups of Hunan Province (No. 2019JJ10001), and Science and Technology Planning Project of Hunan Province (No. 2019RS3010).

n AUTHOR INFORMATION

Corresponding authors. Emails: huagong042cl@163.com (L. Chen), jkguozd@126.com (J. K. Guo) and sf_yin@hnu.edu.cn (S. F. Yin)

n COMPETING INTERESTS

The authors declare no competing financial interest.

n ADDITIONAL INFORMATION

Supplementary information is available for this paper at http://manu30.magtech.com.cn/jghx/EN/10.14102/j.cnki.0254-5861.2022-0149

For submission: https://www.editorialmanager.com/cjschem

n REFERENCES

(1) Shilov, A. E.; Shul'pin, G. B. Activation of C-H bonds by metal complexes. *Chem. Rev.* **1997**, 97, 2879-2932.

(2) Bergman, R. G. C-H activation. *Nature* **2007**, 446, 391-393.

(3) Tripathy, J.; Lee, K.; Schmuki, P. Tuning the selectivity of photocatalytic synthetic reactions using modified TiO_2 nanotubes. *Angew. Chem. Int. Ed.* **2014**, 126, 12813-12816.

(4) Chen, P.; Liu, F.; Ding, H.-Z.; Chen, S.; Chen, L.; Li, Y. J.; Au, C. T.; Yin, S. F. Porous double-shell CdS@C_3N_4 octahedron derived by in situ supramolecular self-assembly for enhanced photocatalytic activity. *Appl. Catal. B: Environ.* **2019**, 252, 33-40.

(5) Balcells, D.; Clot, E.; Eisenstein, O. C-H bond activation in transition metal species from a computational perspective. *Chem. Rev*. **2010**, 110, 749-832.

(6) Kesavan, L.; Tiruvalam, R.; Ab Rahim, M. H.; Bin Saiman, M. I.; Enache, D. I.; Jenkins, R. L.; Dimitratos, N.; Lopez-Sanchez, J. A.; Taylor, S. H.; Knight, D. W. Solvent-free oxidation of primary carbon-hydrogen bonds in toluene using Au-Pd alloy nanoparticles. *Science* **2011**, 331, 195-199.

(7) Fujihira, M.; Satoh, Y.; Osa, T. Heterogeneous photocatalytic oxidation of aromatic compounds on TiO_2. *Nature* **1981**, 293, 206-208.

(8) Cao, X.; Chen, Z.; Lin, R.; Cheong, W. C.; Liu, S.; Zhang, J.; Peng, Q.; Chen, C.; Han, T.; Tong, X. A photochromic composite with enhanced carrier separation for the photocatalytic activation of benzylic C-H bonds in toluene. *Nat. Catal.* **2018**, 1, 704-710.

(9) He, J.; Chen, L.; Ding, D.; Yang, Y. K.; Au, C. T.; Yin, S. F. Facile fabrication of novel $Cd_3(C_3N_3S_3)_2$/CdS porous composites and their photocatalytic performance for toluene selective oxidation under visible light irradiation. *Appl. Catal. B: Environ.* **2018**, 233, 243-249.

(10) Yu, B.; Zhang, S. M.; Wang, X. Helical microporous nanorods assembled by polyoxometalate clusters for the photocatalytic oxidation of toluene. *Angew. Chem. Int. Ed.* **2021**, 60, 17404-17409.

(11) Bai, Z. J.; Tan, X. P.; Chen, L.; Hu, B.; Tan, Y. X.; Mao, Y.; Shen, S.; Guo, J. K.; Au, C. T.; Liang, Z. W.; Yin, S. F. Efficient photocatalytic toluene selective oxidation over $Cs_3Bi_{1.8}Sb_{0.2}Br_9$ nanosheets: enhanced charge carriers generation and C-H bond dissociation. *Chem. Eng. Sci.* **2022**, 247, 116983.

(12) Zhao, Y. Z.; Dai, Y.; Wang, Q. H.; Dong, Y. Y.; Song, T. L.; Mudryi, A.; Chen, Q.; Li, Y. J. Anions-exchange-induced efficient carrier transport at $CsPbBr_xCl_{3-x}/TiO_2$ interface for photocatalytic activation of C(sp^3)-H bond in toluene oxidation. *ChemCatChem* **2021**, 13, 2592-2598.

(13) Tan, Y. X.; Chai, Z. M.; Wang, B. H.; Tian, S.; Deng, X. X.; Bai, Z. J.; Chen, L.; Guo, J. K.; Shen, S.; Cai, M. Q.; Au, C. T.; Yin, S. F. Boosted photocatalytic oxidation of toluene into benzaldehyde on $CdIn_2S_4$-CdS: synergetic effect of compact heterojunction and S-vacancy. *ACS Catal.* **2021**, 11, 2492-2503.

(14) Dai, Y.; Poidevin, C.; Ochoa-Hernández, C.; Auer, A. A.; Tüysüz, H. A supported bismuth halide perovskite photocatalyst for selective aliphatic and aromatic C-H bond activation. *Angew. Chem. Int. Ed*. **2020**, 132, 5837-5845.

DOI: 10.14102/j.cnki.0254-5861.2022-0149

(15) Yuan, R. S.; Fan, S. L.; Zhou, H. X.; Ding, Z. X.; Lin, S.; Li, Z. H.; Zhang, Z. Z.; Chao, X.; Wu, L.; Wang, X. X.; Fu, X. Z. Chlorine-radical-mediated photocatalytic activation of C-H bonds with visible light. *Angew. Chem. Int. Ed*. **2013**, 125, 1069-1073.
(16) Qiu, G. H.; Wang, T.; Li, X. L.; Tao, X. Q.; Li, B. X. Novel BiOCl/$BiCl_3$Br-CTA heterostructure photocatalyst with abundant oxygen vacancies and a superoleophilic surface for promoting selective oxidation of toluene. *Ind. Eng. Chem. Res*. **2020**, 59, 11517-11526.
(17) Deng, X. X.; Tian, S.; Chai, Z. M.; Bai, Z. J.; Tan, Y. X.; Chen, L.; Guo, J. K.; Shen, S.; Cai, M. Q.; Au, C. T.; Yin, S. F. Boosted activity for toluene selective photooxidation over Fe-doped Bi_2WO_6. *Ind. Eng. Chem. Res.* **2020**, 59, 13528-13538.
(18) Xu, C. Y.; Pan, Y. T.; Wan, G.; Liu, H.; Wang, L.; Zhou, H.; Yu, S. H.; Jiang, H. L. Turning on visible-light photocatalytic C-H oxidation over metal-organic frameworks by introducing metal-to-cluster charge transfer. *J. Am. Chem. Soc.* **2019**, 141, 19110-19117.
(19) Chen, L.; Tang, J.; Song, L. N.; Chen, P.; He, J.; Au, C. T.; Yin, S. F. Heterogeneous photocatalysis for selective oxidation of alcohols and hydrocarbons. *Appl. Catal. B: Environ.* **2019**, 242, 379-388.
(20) Li, X. L.; Wang, T.; Tao, X. Q.; Qiu, G. H.; Li, C.; Li, B. X. Interfacial synergy of Pd sites and defective BiOBr for promoting the solar-driven selective oxidation of toluene. *J. Mater. Chem. A* **2020**, 8, 17657-17669.
(21) Huang, H. W.; Yuan, H. F.; Zhao, J. W.; Solis-Fernandez, G.; Zhou, C.; Seo, J. W.; Hendrix, J.; Debroye, E.; Steele, J. A.; Hofkens, J.; Long, J. J.; Roeffaers, M. B. C(sp^3)-H bond activation by perovskite solar photocatalyst cell. *ACS Energy Lett.* **2018**, 4, 203-208.
(22) Li, Y. J.; Li, M.; Xu, P.; Tang, S. H.; Liu, C. Efficient photocatalytic degradation of acid orange 7 over N-doped ordered mesoporous titania on carbon fibers under visible-light irradiation based on three synergistic effects. *Appl. Catal. A-Gen.* **2016**, 524, 163-172.
(23) Liu, F.; Xiao, C. X.; Meng, L. H.; Chen, L.; Zhang, Q.; Liu, J. B.; Shen, S.; Guo, J. K.; Au, C. T.; Yin, S. F. Facile fabrication of octahedral CdS-ZnS by cation exchange for photocatalytic toluene selective oxidation. *ACS Sustain. Chem. Eng.* **2020**, 8, 1302-1310.
(24) Song, L. N.; Chen, L.; He, J.; Chen, P.; Zeng, H. K.; Au, C. T.; Yin, S. F. The first synthesis of Bi self-doped Bi_2MoO_6-$Bi_2Mo_3O_{12}$ composites and their excellent photocatalytic performance for selective oxidation of aromatic alkanes under visible light irradiation. *Chem. Commun*. **2017**, 53, 6480-6483.
(25) Cai, K.; Lv, S. Y.; Song, L. N.; Chen, L.; He, J.; Chen, P.; Au, C. T.; Yin, S. F. Facile preparation of ultrathin Bi_2MoO_6 nanosheets for photocatalytic oxidation of toluene to benzaldehyde under visible light irradiation. *J. Solid State Chem.* **2019**, 269, 145-150
(26) Dai, Z.; Qin, F.; Zhao, H. P.; Ding, J.; Liu, Y. L.; Chen, R. Crystal defect engineering of aurivillius Bi_2MoO_6 by Ce doping for increased reactive species production in photocatalysis. *ACS Catal.* **2016**, 6, 3180-3192.
(27) Zhang, B.; Yang, X.; Li, J.; Cheng, G. Selective aerobic oxidation of alkyl aromatics on Bi_2MoO_6 nanoplates decorated with Pt nanoparticles under visible light irradiation. *Chem. Commun.* **2018**, 54, 12194-12197.
(28) Yang, M.; Wang, P.; Li, Y. J.; Tang, S. P.; Lin, X.; Zhang, H. Y.; Zhu, Z.; Chen, F. T. Graphene aerogel-based NiAl-LDH/g-C_3N_4 with ultratight sheet-sheet heterojunction for excellent visible-light photocatalytic activity of CO_2 reduction. *Appl. Catal. B: Environ.* **2022**, 306, 121065.
(29) Chen, C.; Qiu, G. H.; Wang, T.; Zheng, Z. Q.; Huang, M. T.; Li, B. X. Modulating oxygen vacancies on bismuth-molybdate hierarchical hollow microspheres for photocatalytic selective alcohol oxidation with hydrogen peroxide production. *J. Colloid Interf. Sci.* **2021**, 592, 1-12.
(30) Li, S. J.; Wang, C. C.; Liu, Y. P.; Cai, M. J.; Wang, Y. N.; Guo, Y.; Zhao, W.; Wang, Z. H.; Chen, X. B. Photocatalytic degradation of tetracycline antibiotic by a novel $Bi_2Sn_2O_7$/Bi_2MoO_6 S-scheme heterojunction: performance, mechanism insight, and toxicity assessment. *Chem. Eng. J.* **2022**, 429, 132519.
(31) Wu, Y. L.; Li, Y. J.; Zhang, L. J.; Jin, Z. L. NiAl-LDH in-situ derived Ni_2P and ZnCdS nanoparticles ingeniously constructed S-scheme heterojunction for photocatalytic hydrogen evolution. *ChemCatChem* **2021**, 14, e202101656.
(32) Wang, C. C.; Li, S. J.; Cai, M. J.; Yan, R. Y.; Dong, K. X.; Zhang, J. L.; Liu, Y. P. Rationally designed tetra (4-carboxyphenyl) porphyrin/graphene quantum dots/bismuth molybdate Z-scheme heterojunction for tetracycline degradation and Cr(VI) reduction: performance, mechanism, intermediate toxicity appraisement. *J. Colloid Interf. Sci.* **2022**, 619, 307-321.
(33) Song, L. N.; Ding, F.; Yang, Y. K.; Ding, D.; Chen, L.; Au, C. T.; Yin, S. F. Synthesis of TiO_2/Bi_2MoO_6 composite for partial oxidation of aromatic alkanes under visible-light illumination. *ACS Sustain. Chem. Eng.* **2018**, 6, 17044-17050.
(34) Kan, L.; Yang, L. P.; Mu, W. N.; Wang, Q.; Wang, X. Y.; Chang, C. Facile one-step strategy for the formation of $BiOIO_3$/$[Bi_6O_6(OH)_3]$-$(NO_3)_3$·1.5H_2O heterojunction to enhancing photocatalytic activity. *J. Colloid Interf. Sci.* **2022**, 612, 401-412.
(35) Pang, J. W.; Han, Q. F.; Liu, W. Q.; Shen, Z. C.; Wang, X.; Zhu, J. W. Two basic bismuth nitrates: $[Bi_6O_6(OH)_2](NO_3)_4$·2H_2O with superior photodegradation activity for rhodamine B and $[Bi_6O_5(OH)_3](NO_3)_5$·3H_2O with ultrahigh adsorption capacity for methyl orange. *Appl. Surf. Sci.* **2017**, 422, 283-294.
(36) Wu, X. L.; Ng, Y. H.; Wen, X. M.; Chung, H. Y.; Wong, R. J.; Du, Y.; Dou, S. X.; Amal, R. Scott, J. Construction of a Bi_2MoO_6:$Bi_2Mo_3O_{12}$ heterojunction for efficient photocatalytic oxygen evolution. *Chem. Eng. J.* **2018**, 353, 636-644.
(37) Ma, Y. Y.; Han, Q. F.; Wang, X.; Zhu, J. W. An in situ annealing route to $[Bi_6O_6(OH)_2](NO_3)_4$·2H_2O/g-C_3N_4 heterojunction and its visible-light-driven photocatalytic performance. *Mater. Res. Bull*. **2018**, 101, 272-279.
(38) Sun, S. C.; Zhou, W. M.; Wang, L. Y.; Zhang, M. X.; Lawan, I.; Wang, L. W.; Zhang F.; Lin, M.; Yuan, Z. H. Oxygen-vacancy engineering approach to bismuth basic nitrate/g-C_3N_4 heterostructure for efficiently photocatalytic hydrogen evolution. *Int. J. Hydrogen Energy* **2021**, 46, 25832-25842.
(39) Li, Q. L.; Song, T.; Zhang, Y. P.; Wang, Q.; Yang, Y. Boosting photocatalytic activity and stability of lead-free $Cs_3Bi_2Br_9$ perovskite nanocrystals via in situ growth on monolayer 2D $Ti_3C_2T_x$ MXene for C-H bond oxidation. *ACS Appl. Mater. Interfaces* **2021**, 13, 27323-27333.
(40) Li, S. J.; Wang, C. C.; Cai, M. J.; Yang, F.; Liu, Y. P.; Chen, J. L.; Zhang, P.; Li, X.; Chen, X. B. Facile fabrication of TaON/Bi_2MoO_6 core-shell S-scheme heterojunction nanofibers for boosting visible-light catalytic levofloxacin degradation and Cr (VI) reduction. *Chem. Eng. J.* **2022**, 428, 131158.
(41) Guo, J. H.; Shi, L.; Zhao, J. Y.; Wang, Y.; Tang, K. B.; Zhang, W. Q.; Xie, C. Z.; Yuan, X. Y. Enhanced visible-light photocatalytic activity of Bi_2MoO_6 nanoplates with heterogeneous Bi_2MoO_{6-x}@Bi_2MoO_6 core-shell structure. *Appl. Catal. B: Environ.* **2018**, 224, 692-704.
(42) Li, S. J.; Wang, C. C.; Cai, M. J.; Liu, Y. P.; Wang, Y. N.; Dong, K. E.; Zhang, J. L. Designing oxygen vacancy mediated bismuth molybdate (Bi_2MoO_6)/N-rich carbon nitride (C_3N_5) S-scheme heterojunctions for

DOI: 10.14102/j.cnki.0254-5861.2022-0149

boosted photocatalytic removal of tetracycline antibiotic and Cr (VI): intermediate toxicity and mechanism insight. *J. Colloid Interf. Sci.* **2022**, 624, 219-232.

(43) Zhang, H.; Guo, L. H.; Zhao, L. X.; Wan, B.; Yang, Y. Switching oxygen reduction pathway by exfoliating graphitic carbon nitride for enhanced photocatalytic phenol degradation. *J. Phys. Chem. Lett.* **2015**, 6, 958-963.

(44) Chai, Z. M.; Wang, B. H.; Tan, Y. X.; Bai, Z. J.; Pan, J. B.; Chen, L.; Shen, S.; Cai, M. Q.; Au, C. T.; Yin, S. F. Enhanced photocatalytic activity for selective oxidation of toluene over cubic-hexagonal CdS phase junctions. *Ind. Eng. Chem. Res.* **2021**, 60, 11106-11116.

(45) Sun, X.; Luo, X.; Zhang, X.; Xie, J.; Jin, S.; Wang, H.; Zheng, X.; Wu, X.; Xie, Y. Enhanced superoxide generation on defective surfaces for selective photocatalytic oxidation. *J. Am. Chem. Soc.* **2019**, 141, 3797-3801.

(46) Tamai, K.; Murakami, K.; Hosokawa, S.; Asakura, H.; Teramura, K.; Tanaka, T. Visible-light selective photooxidation of aromatic hydrocarbons via ligand-to-metal charge transfer transition on Nb_2O_5. *J. Phys. Chem. C* **2017**, 121, 22854-22861.

(47) Su, K. Y.; Liu, H. F.; Zeng, B.; Zhang, Z. X.; Luo, N. C.; Huang, Z. P.; Gao, Z. Y.; Wang, F. Visible-light-driven selective oxidation of toluene into benzaldehyde over nitrogen-modified Nb_2O_5 nanomeshes. *ACS Catal.* **2020**, 10, 1324-1333.

(48) Dai, Y.; Tüysüz, H. Rapid acidic media growth of $Cs_3Bi_2Br_9$ halide perovskite platelets for photocatalytic toluene oxidation. *Sol. RRL* **2021**, 5, 2100265.

(49) Zhang, Z. Z.; Yang, Y. Y.; Wang, Y. Y.; Yang, L. L.; Li, Q.; Chen, L. X.; Xu, D. S. Revealing the A-site effect of lead-free $A_3Sb_2Br_9$ perovskite in photocatalytic C(sp^3)-H bond activation. *Angew. Chem. Int. Ed.* **2020**, 132, 18293-18296.

(50) Nadimicherla, R.; Zha, R. H.; Wei, L.; Guo, X. Single crystalline flower-like α-MoO_3 nanorods and their application as anode material for lithium-ion batteries. *J. Alloys Compd.* **2016**, 687, 79-86.

(51) Li, Y. J.; Chen, W.; Li, L. Y.; Ma, M. Y. Photoactivity of titanium dioxide/carbon felt composites prepared with the assistance of supercritical carbon dioxide: effects of calcination temperature and supercritical conditions. *Sci. China Chem.* **2011**, 54, 497-505.

Received: June 6, 2022
Accepted: June 29, 2022
Published online: July 4, 2022
Published: December 2, 2022

DOI: 10.14102/j.cnki.0254-5861.2022-0149